DEUTSCHES ELEKTRONEN – SYNCHROTRON

DESY 93-010
January 1993

Single Jet Photoproduction at HERA in Next-to-Leading Order QCD

G. Kramer, S. G. Salesch

II. Institut für Theoretische Physik, Universität Hamburg

ISSN 0418-9833

NOTKESTRASSE 85 · D-2000 HAMBURG 52

To be sure that your preprints are promptly included in the
HIGH ENERGY PHYSICS INDEX,
send them to (if possible by air mail):

DESY **Bibliothek** **Notkestraße 85** **W-2000 Hamburg 52** **Germany**	**DESY-IfH** **Bibliothek** **Platanenallee 6** **O-1615 Zeuthen** **Germany**

DESY 93-010
January 1993

ISSN 0418-9833

Single Jet Photoproduction at HERA in Next-to-Leading Order QCD

G. KRAMER AND S.G. SALESCH
II. INSTITUT FÜR THEORETISCHE PHYSIK* DER UNIVERSITÄT HAMBURG,
LURUPER CHAUSSEE 149, DW - 2000 HAMBURG 50

January 1993

Abstract

We present results for next-to-leading order calculations of single jet inclusive cross sections by resolved photons in ep-collisions at HERA . The dependence on the jet recombination cut and on the choice of the renormalization and factorization scales is studied in detail.

*Supported by Bundesministerium für Forschung und Technologie, 055HH91P(8), Bonn, FRG

1 Introduction

The production of high transverse momentum (p_T) jets by quasi-real photons, emitted by the electron beam, on protons is one of the major processes to gain information on the quark and in particular the gluon structure of the photon. First results by the ZEUS and H1 collaborations at HERA have been presented recently [1,2]. These first data have been compared already with theoretical cross sections obtained in leading order (LO) in QCD. As is well known such leading order estimates suffer from normalization uncertanties due to the renormalization / factorization scale dependence. In addition such cross sections have no dependence on the jet resolution parameter, for example the cone size R. To severely constrain the photon structure function the knowledge of higher-order QCD corrections is mandatory.

There are two types of mechanisms which contribute to the photoproduction of jets at high energies. The photon can interact directly or via its quark and gluon content, the so-called *resolved* part, with the partons coming out of the proton and so producing high-p_T jets. The lowest order term of the direct contribution is of $\mathcal{O}(\alpha\alpha_s)$ whereas the parton-parton scattering term induced by the resolved photon is of $\mathcal{O}(\alpha_s^2)$. Since the latter one is multiplied by the photon structure function which has a contribution of $\mathcal{O}(\alpha/\alpha_s)$, both contributions are of the same order in a pertubative expansion [3,4,5]. Actually, the resolved photoproduction dominates at HERA energies for small p_T and negative rapidities (our definition of the pseudorapidity η follows [3], the direction of the incoming electron defines $\eta_{Lab} > 0$) [3,4,5,6]. Near the maximum of the rapidity distribution ($\eta_{Lab} \simeq -2$) the resolved and the direct part become comparable at $p_T \simeq 35$ GeV. So either by appropriate kinematical cuts in p_T and η_{Lab} or by observing the remnants of the resolved photon near the beam pipe it is feasible to obtain information on the resolved part alone [7]. Furthermore recent data from H1 and ZEUS indicate that the resolved production of jets dominates at small p_T [1,2]. Thus considering resolved photoproduction as a seperate process it is important to obtain predictions as reliable as possible. For this goal we have calculated next-to-leading order (NLO) corrections just for resolved photoproduction. Results for NLO corrections to direct photoproduction of jets have been presented recently by Bödeker [8] and will be of interest in the positive η_{Lab} or/and large transverse momentum region.

To perform a consistent calculation of single jet inclusive production in the NLO formalism we need the NLO hard scattering cross section with two-loop $\alpha_s(\mu)$ and two-loop evolved structure functions of the photon and the proton. Only under these circumstances all three elements are unambiguously defined. NLO parametrizations of the proton exist for some time [9,10]. Recently three sets of NLO parametrizations of the parton distributions of the photon have appeared in the literature [11,12,13]. They have been tested against the available experimental data on the photon structure function $\mathcal{F}_2^\gamma(x,Q^2)$. The NLO corrections to the hard scattering parton-parton cross sections have been worked out by Aversa et. al.[14] and Ellis et al.[15] using two completely different schemes. In the work of Aversa et al., which was applied to single inclusive jet production in $p\bar{p}$- and pp-collisions, the two jet production up to $\mathcal{O}(\alpha_s^3)$ is calculated in the small-cone approximation (SCA) analytically. The extension to finite cone sizes can be found in [16]. This is based on Monte Carlo integrations using the known $2\rightarrow 3$ parton cross sections. The calculation of Ellis et al., on the other hand, is completely analytical for all cone sizes up to $\pi/3$. We have done similar calculations for γp reactions with resolved photons in the HERA energy regime by using the method of Aversa et al..

In sect.2 we describe our theoretical input concerning structure functions and hard scattering matrix elements. The main results are presented in sect.3. There we consider in particular the influence of the NLO corrections, the cone size dependence and the influence of scale variations on the final result. Some of these results using the SCA and LO photon structure functions have been reported earlier [17]. When completing the work presented here we received the short note of Gordon and Storrow [18] in which results on NLO cross sections for direct and resolved photoproduction are reported. Whenever possible we shall compare with these results.

2 Theoretical Ingredients

We consider only the resolved photon, although for a complete description in all kinematical regions and without observing the photon remnants [1,2] the direct photon contribution must be included. This is left for the future. The photon emission from the electron is described in the Weizsäcker-Williams equivalent photon approximation with an angle cut of 5^o for the final state electron with a formula as in [3]. We calculated our cross sections with an electron energy of $p_e = 30\,GeV$ and a proton energy of $p_p = 820\,GeV$, resulting in $\sqrt{S_{\mathrm{HERA}}} = 314\,GeV$. For our NLO calculations we present results only for one combination of parton distribution functions for the proton *and* the photon. For the proton we have chosen the B1 set of Morfin and Tung [9] in the $\overline{MS}$ factorization scheme. The photon structure functions are taken from the paper of Glück, Reya and Vogt [11], also in the $\overline{MS}$ scheme. Both are NLO parametrizations. In ref.[11] another NLO photon structure function, in the so-called DIS_γ scheme, can be found, but we shall not use it here. For $\alpha_s(\mu)$ both in one- and two-loop approximation we employ the formulas of [19] with $N_f = 4$ active flavours and the QCD scale parameter given by the *proton* structure function, i.e. $\Lambda = 194\,MeV$ for MT, set B1 [9]. We note that the NLO structure function of GRV [11] has an only slightly larger $\Lambda = 200\,MeV$ ($N_f = 4$) so our choice should be a consistent one.
When comparing to lowest order (Born cross sections) we introduce the one-loop coupling but retain the NLO parton distributions to get a feeling of the NLO corrections of the hard scattering process. Of course, to see the whole effect of the higher order QCD corrections we should compare to a *bona fide* Born cross section based on LO structure functions both for the proton and the photon. Therefore we give results of both types of Born calculations at the end.
Primarily we adopted the jet definition proposed by the Snowmass Meeting 1990 [20]. According to the Snowmass Accord a jet is defined as transverse *energy* (rather than momentum) deposited in a cone of radius R in the pseudorapidity–azimuthal angle (η, Φ)–plane. The jet axis (η_J, Φ_J) is defined as

$$E_T(\eta_J, \Phi_J) = \sum_{i \in Jet} E_{T,i}(\eta_i, \Phi_i) \tag{1}$$

with the jet transverse energy

$$E_T = \sum_{i \in Jet} E_{T,i}\,. \tag{2}$$

In the following the transverse energy of a Snowmass jet will be denoted as p_T. A parton with kinematical variables (η_i, Φ_i) is included in the jet if

$$(\Phi_i - \Phi_J)^2 + (\eta_i - \eta_J)^2 \leq R^2 \tag{3}$$

is satisfied. For 2→3 processes not more than two partons can build up a jet defined this way. In contrast to eqns.(1) and (2), CDF defines the jet 4-momentum as a sum over the 4-momenta of the particles included in a cone of size R in the (η, Φ)–plane. So, in the context of the CDF jet definition, the transverse momentum is well defined and will be denoted here as p_T, too, to simplify our notations.

The hard scattering part for inclusive single jet production in $\mathcal{O}(\alpha_s^3)$ were calculated with the help of a routine developed by Aversa et al.[14]. To cancel the infrared and collinear divergencies in the final state they combined those 2→3 configurations where two partons have their 3–momenta within a cone of opening angle 2δ centered at the jet 3–momentum, with the virtual corrections to the 2→2 processes. This could be done analytically for small cone sizes and large scattering angles, equivalent to the restriction

$$\delta \cdot \cosh(\eta_J) \ll 1 \tag{4}$$

In the range of validity of eqn.(4) their definition of a jet can be identified with the Snowmass Accord using

$$R = \delta \cdot \cosh(\eta_J) + \mathcal{O}(\delta^2) \tag{5}$$

Note that both δ and η_J are clearly not independent under boosts along the ep-beam axis, while the combination R is.
Although these formulas are not applicable for large δ and/or large rapidities, their universal feature allows for the calculation of the correct finite cone behaviour of various jet definitions by adding the well defined corrections. To obtain results for experimentally relevant large opening angles δ or cone sizes R the cross section for a cone of any size was evaluated by adding the contributions of unresolved partons in the *crown* between the cones of opening angle $2\delta_0$ and cone size R. This can be done numerically using the known matrix elements for 2→3 processes [21,22]. The following channels contribute in $\mathcal{O}(\alpha_s^3)$

$$\begin{aligned}
q_i + q_k &\longrightarrow q_i + q_k + G \\
q_i + \bar{q}_k &\longrightarrow q_i + \bar{q}_k + G \\
q_i + q_i &\longrightarrow q_i + q_i + G \\
q_i + \bar{q}_i &\longrightarrow \begin{cases} q_i + \bar{q}_i + G \\ q_k + \bar{q}_k + G \\ G + G + G \end{cases} \\
q_i + G &\longrightarrow \begin{cases} q_i + G + G \\ q_i + q_i + \bar{q}_i \\ q_i + q_k + \bar{q}_k \end{cases} \\
G + G &\longrightarrow \begin{cases} G + G + G \\ q_i + \bar{q}_i + G \end{cases}
\end{aligned} \tag{6}$$

We choose both the renormalization scale μ and the factorization scale Q in the photon and the proton structure function equal to p_T : $\mu = Q = p_T$.

3 Results

To get an overview we first show the p_T distribution near the maximum of the rapidity distribution, i.e. at η_{Lab} =−3, −2 and −1, in Fig.1. This plot gives $d^2\sigma/d\eta\, dp_T$ as a function of p_T for the complete theory up to $\mathcal{O}(\alpha_s^3)$ with cone size $R = 1$. We see that the cross section falls off with increasing p_T rather strongly. The even stronger decrease at η_{Lab} =−3 is caused by the phase space limit while the maximum of the rapidity distribution is located between η_{Lab} =−2 and η_{Lab} =−1 moving along the direction of the incident electron beam with increasing p_T . This behaviour is already present in the Born approximation not shown here. In Fig.2 we compare the cross section $d^2\sigma/d\eta\, dp_T$ for two different jet recombination schemes, the Snowmass Accord and the CDF jet definition[20], respectively, with $R = 1$ at η_{Lab} =−2. On the logarithmic plot the difference between these two jet definitions appears to be small, i.e. of the order of 10% over the whole range of p_T . This can be seen explicitly in the rightmost column in Tab.1 where the ratios of these cross sections are given. These numbers should be accurate on a 1% -level. In Fig.2 we also show the LO cross section (labelled Born) in the definition introduced in sect.2, i.e. with the same structure functions as in the NLO evaluation, but $\alpha_s(\mu)$ and the hard parton-parton cross section in lowest order. We see that the full cross section is about 20% larger than the Born result. This increase is very similar for η_{Lab} =−1. Increasing p_T up to 50 GeV, η_{Lab} =−3 approaches the edge of phase space which causes a somewhat different behaviour at this rapidity. A list of these ratios, i.e. for η_{Lab} =−1,−2 and −3, is presented on the left hand side of Tab.1.

The NLO results in Figs.1 and 2 and in the following are all obtained by calculating the SCA cross section analytically [14] with a cone size of $\delta_0 = 0.01$ in the ep–center-of-mass system and adding the numerically calculated contribution to correct for the finite jet cut. We checked the stability of our results by varying δ_0 up to 0.10 – within the range of validity of the SCA – and found the final results to be independent of δ_0 within the statistical errors of our integration routines.

The cross section $d^2\sigma/d\eta\, dp_T$ as a function of η_{Lab} for $p_T = 5, 15$ and $50\,GeV$ is plotted in Fig.3a,b,c , respectively. The (Snowmass) cone radii are $R = 0.7$ and 1.0. As an example, the SCA cross section for $\delta = 0.01$ is plotted, too. Note, that this curve corresponds to cross sections with *variable* cone size R according to eqn.(5). The jet opening angle δ in this paper is always defined in the ep–center-of-mass system. At such small cone sizes the rapidity distribution shows an interesting structure, unfortunately the corresponding jets cannot be constructed experimentally. The curve with $R = 0.7$ almost coincides with the Born cross section for $p_T = 5$ and $15\,GeV$. At $p_T = 50\,GeV$ this occurs at a somewhat lower $R \simeq 0.6$, which is shown in Fig.3c. From these plots we conclude that the cone dependence of the cross section as a function of p_T and/or η_{Lab} is the most interesting feature where the NLO corrections in the hard scattering show up, completely analogous to studies in purely hadronic reactions like pp and $p\bar{p}$ scattering [14,15,16].
For small cone sizes we expect the dependence on R to be like $a + b \log R$. For larger radii deviations from this simple behaviour occur. This is exhibited in Fig.4a,b,c where the cone dependence of $d^2\sigma/d\eta\, dp_T$ at η_{Lab} =−2 is shown for $p_T = 5$, 15 and $50\,GeV$. For $p_T \leq 15\,GeV$ the $\log R$ dependence already breaks down for $R \geq 0.3$ in such a way that the cross section is larger above this value of R as compared to the SCA. At $R = 1$, the Snowmass Accord leads

approximately to a 20%, the CDF jet definition to a 10% deviation from the SCA result. This difference decreases with increasing p_T , at $p_T = 50\,GeV$ the small-cone approximation is acceptable up to $R \simeq 0.4$. The stronger deviation of the Snowmass cross section is partly due to the fact that the ratio of the jet transverse energy over the jet transverse momentum behaves like $1 + \mathcal{O}(R^2)$. In other words, the difference between cross sections using the Snowmass and the CDF jet definitions, respectively, should decrease when looking at the transverse *energy* only. Nevertheless, we think that our choice of cross sections gives a good hint on the influence of different jet definitions on NLO jet cross sections.

It is clear that the variation of the cross section with R must depend on the value of $\Lambda_{\overline{MS}}$. The larger the higher order correction the stronger the dependence on the cone size.

As another important point in connection with NLO corrections we consider the scale dependence of the cross section $d^2\sigma/d\eta\, dp_T$. In Fig.5 we show the cross section plotted as a function of $\xi = \mu/p_T = Q/p_T$ in the range between $0.5 \leq \xi \leq 8.0$ at $p_T = 5\,GeV$ and $0.25 \leq \xi \leq 4.0$ at $p_T = 15,\ 50\,GeV$, at $\eta_{Lab} = -2$. As expected, the NLO cross sections with finite cone sizes ($R = 0.7, 1.0$) are much less scale dependent than the Born cross section. We also show the scale dependence for the small cone size $\delta = 0.01$, which is completely different from the one at large cones. This is due to the strong influence of the negative virtual corrections. With increasing cone size the contribution of the real 2→3 corrections become more and more important. One has to keep in mind that the hard scattering part of the finite cone corrections is build up from the 2→3 *tree* graph contributions which have no pieces compensating the scale dependence. At larger R, this clearly must lead to a scale dependence rather similar to the one of the Born cross section. Interpolating between the curves with $\delta = 0.01$ and $R = 1$, respectively, suggests that an *optimum jet cone size* exists which leads to a very flat scale dependence over a large range in μ, Q. As Fig.5a,b,c tell us, $R = 0.7$ might be such a *best choice*. Nevertheless, in the whole range of experimentally accessible jet cone sizes, i.e. $R = 0.1, \ldots, 1.0$, the scale dependence is reduced appreciably. The reduction is largest at largest p_T .

As our last point we come back to the definition of Born cross sections, especially the influence of the choice of different parton distributions in the photon and the proton on the result. As an example, in Tab.2 ratios of our standard Born cross section evaluated with NLO parametrizations, to a LO cross section evaluated using the GRV(LO) [11] and the MT(S, LO) [9] parametrizations for the photon and the proton, respectively, are shown. 'Our' Born cross section appears to be about 10% to 50% larger, strongly depending on p_T , than the *bona fide* cross section. This strong effect is only partly caused by the uncertainty due to the QCD scale. The pure LO Born cross section has been calculated with $\Lambda = 144\,MeV$ as required by the MT(S, LO) structure function. In the rightmost column of Tab.2 we show the ratio of the corresponding running couplings squared, i.e.

$$(\alpha_S(\mu = p_T, \Lambda_{MT(B1)})/\alpha_S(\mu = p_T, \Lambda_{MT(S,LO)}))^2 \qquad (7)$$

which could be factored out of the ratio of the cross sections. This means that between 19% and 11% of this ratio of Born cross sections is caused by the change of Λ values, $\Lambda = 194\,GeV$ (MT(B1)) versus $\Lambda = 144\,GeV$ (MT(S,LO)). Compared to the ratio NLO/Born in Tab.1, which is approximately constant ($\simeq 1.2$) over the whole range of p_T , the ratio NLO/Born

(with Born calculated using *leading order* parton distributions) seems to increase with increasing p_T . The ratio of Born cross sections in Tab.2 can be split into two factors. If we change only the proton function from NLO to LO the ratio varies between 1.10 and 1.18 with increasing p_T and between 0.99 and 1.25 when the GRV(NLO) set is substituted by the LO GRV set. The larger ratio at larger p_T is caused by the fact that we used the $\overline{MS}$ version of GRV(NLO). For the DIS_γ version the increase is reduced roughly by a factor of two. This difference reflects the ambiguity in the choice of the factorization scheme for the photon structure functions. It occurs mostly at high p_T , where the direct contribution becomes important.

Similar calculations as presented here have been done by Gordon and Storrow [18]. On the qualitative level their results are similar to ours. In particular they found a very flat scale dependence at $R = 0.7$ ($p_T = 15GeV, \eta_{Lab} = -2$) in good agreement with our Fig.5b. The deviation of the $\log R$ behaviour they calculated is somewhat stronger than what we found, but still qualitatively similar. Clearly, the different choices of parton distributions in the proton and, in particular, the photon they made should be responsible for a large part of the differences mentioned. But on a more quantitative level a comparison is not easily possible because in [18] the Weizsäcker-Williams approximation used is not specified in detail.

A remark should be added concerning the *wriggles* shown in some curves in Figs.4,5. To keep the amount of used CPU time at a reasonable level, only up to 10 points per curve are calculated using our main FORTRAN code. Finally a standard *interpolation* routine was applied to this set of points, leading sometimes to the mentioned spurious wriggles.

4 Summary

We presented results for single-jet inclusive cross sections in resolved photoproduction for HERA in next-to-leading order QCD. The behaviour of different jet definitions was studied and compared to leading order cross sections.
Taking a jet cone size of $R = 1$, the NLO cross section $d^2\sigma/d\eta\, dp_T$ is found to be roughly 20% larger than the Born cross section when both are calculated using the same NLO combination of parton distribution functions. But, in particular at the wings of the η distribution this ratio depends on the jet rapidity. Clearly the NLO corrections depend on the cone size. At $R \simeq 0.7$ the NLO cross section appears to be approximately equal to the Born result over the whole (p_T , η)–range examined. In the vicinity of the maximum of the η distribution we found the pure $\log R$ dependence of the small-cone approximation to be accurate up to $R \simeq 0.3$, slightly increasing with p_T. An $\mathcal{O}(R^2)$ deviation from this behaviour emerges when using the Snowmass jet definition, ending up in a difference of about 20% to the SCA cross section at $R = 1$. The CDF definition shows a similar picture but a quantitatively smaller deviation from the $\log R$ dependence.
The scale dependence is strongly reduced when adding the NLO corrections and looking at experimentally relevant jet cone sizes, even an *optimum* cone size exists which leads to a very flat dependence on the scales μ and Q. In the maximum of the rapidity distribution this *best choice* is located near $R \simeq 0.7$ over the whole range of p_T examined.
The influence of the choice of structure functions on the (Born) result is not negligible, so care must be taken when defining ratios of NLO over Born cross sections, i.e. K-factors.

Acknowledgement We thank J.Ph. Guillet for providing us with a Fortran code of the results of ref.[14]. Discussions with D. Bödeker and B. Kniehl are gratefully acknowledged.

References

1. ZEUS Collaboration, M. Derrick et al., DESY 92-138
2. H1 Collaboration, T. Ahmed et al., Phys. Lett. **B297**(1992), 205
3. H. Baer, J. Ohnemus, J. F. Owens, Z. Phys. **C42**(1989), 657
4. M. Drees, R. M. Godbole, Phys. Rev. Lett. **61**(1988), 682
5. W. J. Stirling, Z. Kunszt, Proc. HERA Workshop, Hamburg 1987, Vol.1, 331 (edited by R. D. Peccei)
6. M. Drees, R. M. Godbole, Phys. Rev. **D39**(1989), 169;
   see also: H. Baer, J. Ohnemus, J. F. Owens, Phys. Rev. **D40**(1989), 2844
7. G. D'Agostini, D. Monaldi, Proc. *Physics at HERA* Workshop, Hamburg 1991, Vol.1, 527 (edited by W. Buchmüller and G. Ingelman)
8. D. Bödeker, Phys. Lett. **B292**(1992), 164
9. J. G. Morfin, Wu-Ki Tung, Z. Phys. **C52**(1991), 13
10. A. D. Martin, R. G. Roberts, W. J. Stirling,
    Phys. Rev. **D37**(1988), 1161 and Mod. Phys. Lett.**A4**(1989), 1135;
    P. N. Harriman, A. D. Martin, R. G. Roberts, W. J. Stirling, Phys. Rev. **D42**(1990), 798;
    J. Kwiecinski, A. D. Martin, R. G. Roberts, W. J. Stirling, Phys. Rev. **D42**(1990), 3645;
    A. D. Martin, W. J. Stirling, R. G. Roberts, University of Durham preprint, RAL-92-021, DTP/92/16 (1992)
11. M. Glück, E. Reya, A. Vogt, Phys. Rev. **D45**(1992), 3986; Phys. Rev. **D46**(1992), 1973
12. L. E. Gordon, J. K. Storrow, Z. Phys. **C56**(1992), 307
13. P. Aurenche, P. Chiappetta, M. Fontannaz, J. Ph. Guillet, E. Pilon, Orsay preprint, LPTHE Orsay 92/13, ENSLAPP-A-387/92 (1992), to be published in Z. Phys. C .
14. F. Aversa, P. Chiappetta, M. Greco, J. Ph. Guillet,
    Nucl. Phys. **B327**(1989), 105; Z. Phys. **C46**(1990), 253

15. S.D. Ellis, Z. Kunszt, D.E. Soper,
Phys. Rev. Lett. **62**(1989), 726; Phys. Rev. **D40**(1989), 2188

16. F. Aversa, P. Chiappetta, L. Gonzales, M. Greco, J. Ph. Guillet, Z. Phys. **C49**(1991), 459

17. G. Kramer, S.G. Salesch, Proc. *Physics at HERA* Workshop, Hamburg 1991, Vol.1, 649 (edited by W. Buchmüller and G. Ingelman)

18. L.E. Gordon, J.K. Storrow, Phys. Lett. **B291**(1992), 320

19. Review of Particle Properties, Phys. Rev. **D45**(1992), S1

20. J.E. Huth et al., FERMILAB-Conf-90/249-E (1990)

21. F.A. Berends et. al., Phys. Lett. **B103**(1981), 124

22. R.K. Ellis, J.C. Sexton, Nucl. Phys. **B269**(1986), 445

Table Captions

Tab. 1: Ratios of $d^2\sigma/d\eta\, dp_T$. The left part of the table shows the ratio of the NLO cross section at three different rapidities, using the Snowmass jet definition with $R = 1$, to the Born result, obtained with the same (NLO) parton distributions as used in the NLO calculations; the rightmost column contains ratios of NLO cross sections for Snowmass vs. CDF definition, both with $R = 1$ and η_{Lab} =−2.

Tab. 2: In the inner column the ratio between our standard Born cross section $d^2\sigma/d\eta\, dp_T$ with NLO parton distributions and a LO calculation with completely LO input (see text) is shown for various p_T at η_{Lab} =−2. The rightmost column contains the squared ratio of the corresponding running couplings, c.f. eqn.(7).

Figure Captions

Fig. 1: p_T-dependence of the full NLO cross section at $R = 1$ and different rapidities: η_{Lab} =-1 (full line), η_{Lab} =-2 (dotted line) and η_{Lab} =-3 (dashed line).

Fig. 2: Comparison of the Born cross section (full line) with NLO cross sections as a function of p_T with R=1 and Snowmass definition (dashed line) and CDF definition (dotted line) for η_{Lab} =-2.

Fig. 3: Cross section $d^2\sigma/d\eta\, dp_T$ as a function of η_{Lab} .
(a) $p_T = 5\,GeV$. Shown are the Born results (full line) and NLO results for different jet cone sizes R=1 (dashed), R=0.7 (dotted) and δ=0.01 (dash-dotted).
(b) as Fig.3a, but $p_T = 15GeV$.
(c) as Fig.3a, but $p_T = 50GeV$ and R=0.6 instead of R=0.7.

Fig. 4: Dependence on the jet cone size R for different p_T and η_{Lab} =-2.
(a) $p_T = 5\,GeV$. Shown are the Born result (dashed) and NLO results for different jet definitions: Snowmass (full line) and CDF (dotted).
(b) as Fig.4a, but $p_T = 15\,GeV$.
(c) as Fig.4a, but $p_T = 50\,GeV$.

Fig. 5: Scale dependence for different p_T and η_{Lab} =-2, $\xi = \mu/p_T = Q/p_T$.
(a) $p_T = 5\,GeV$. Shown are the Born result (full line) and NLO results for CDF jet definition with R=1 (dash-dotted line) and Snowmass definition with R=1 (upper dashed line) and R=0.7 (lower dashed line); the dotted line shows the SCA result for δ=0.01.
(b) as Fig.5a, but $p_T = 15\,GeV$; no CDF cross section.
(c) as Fig.5b, but $p_T = 50GeV$ and R=0.6 instead of R=0.7.

Tables

p_T	NLO / Born			SM / CDF
(GeV)	η_{Lab} =-3	η_{Lab} =-2	η_{Lab} =-1	η_{Lab} =-2
5	1.17	1.22	1.19	1.12
7.5	1.17	1.21	1.17	1.10
10	1.16	1.18	1.20	1.08
12.5	1.18	1.21	1.18	1.11
15	1.15	1.19	1.20	1.08
20	1.16	1.19	1.19	1.09
25	1.14	1.21	1.20	1.09
30	1.14	1.19	1.21	1.07
40	1.09	1.21	1.21	1.08
50	1.06	1.23	1.23	1.10

Tab.1

p_T	ratio of LO	
(GeV)	cross sections	couplings
5	1.09	1.192
7.5	1.16	1.170
10	1.21	1.157
12.5	1.24	1.148
15	1.26	1.142
20	1.32	1.133
25	1.37	1.126
30	1.41	1.122
40	1.45	1.115
50	1.47	1.110

Tab.2

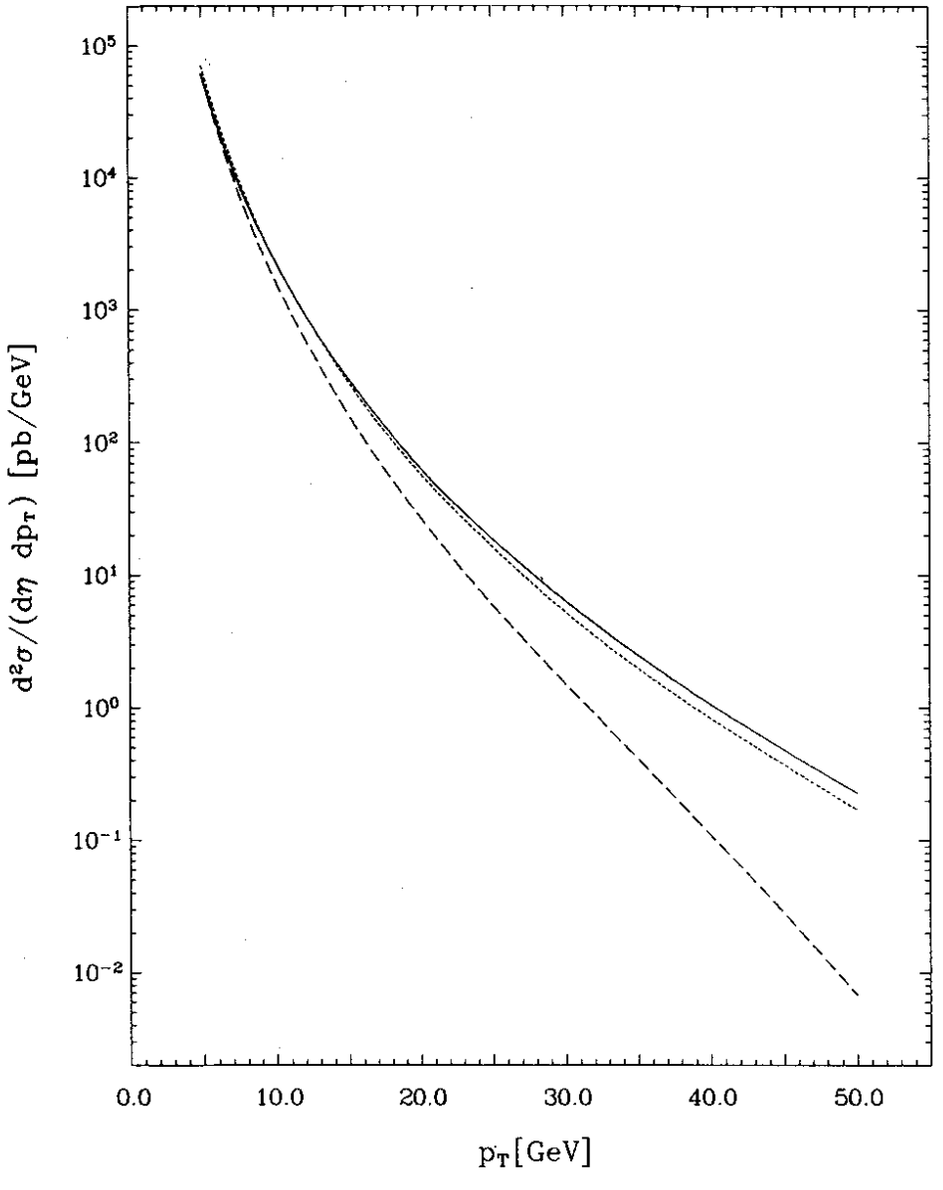
$d^2\sigma/(d\eta\ dp_T)$ [pb/GeV]
10^5
10^4
10^3
10^2
10^1
10^0
10^{-1}
10^{-2}
0.0
10.0
20.0
30.0
40.0
50.0
p_T[GeV]

Fig. 1

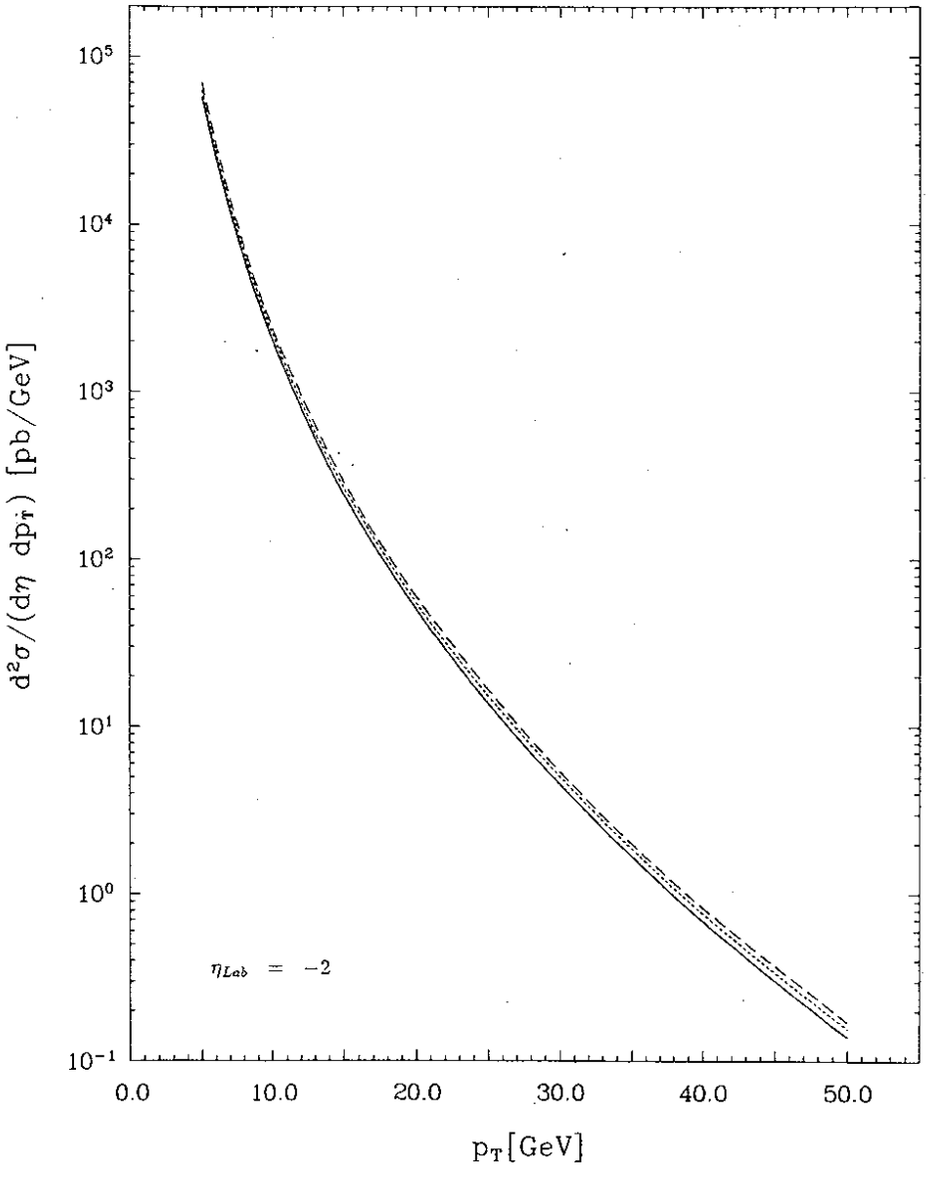
$d^2\sigma/(d\eta\ dp_T)$ [pb/GeV]
10^5
10^4
10^3
10^2
10^1
10^0
10^{-1}
$\eta_{Lab} = -2$
0.0
10.0
20.0
30.0
40.0
50.0
p_T[GeV]

Fig. 2

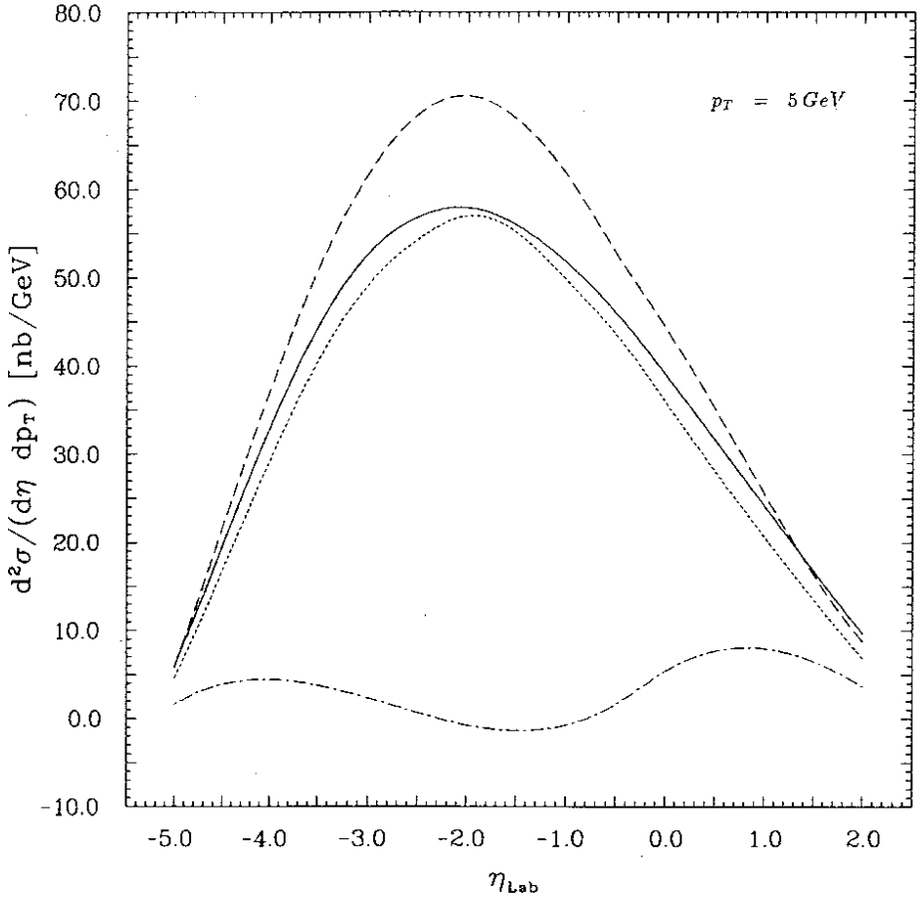
80.0
70.0
60.0
50.0
40.0
30.0
20.0
10.0
0.0
-10.0
-5.0
-4.0
-3.0
-2.0
-1.0
0.0
1.0
2.0
$p_T = 5\,GeV$
$d^2\sigma/(d\eta\ dp_T)$ [nb/GeV]
η_{Lab}

Fig. 3a

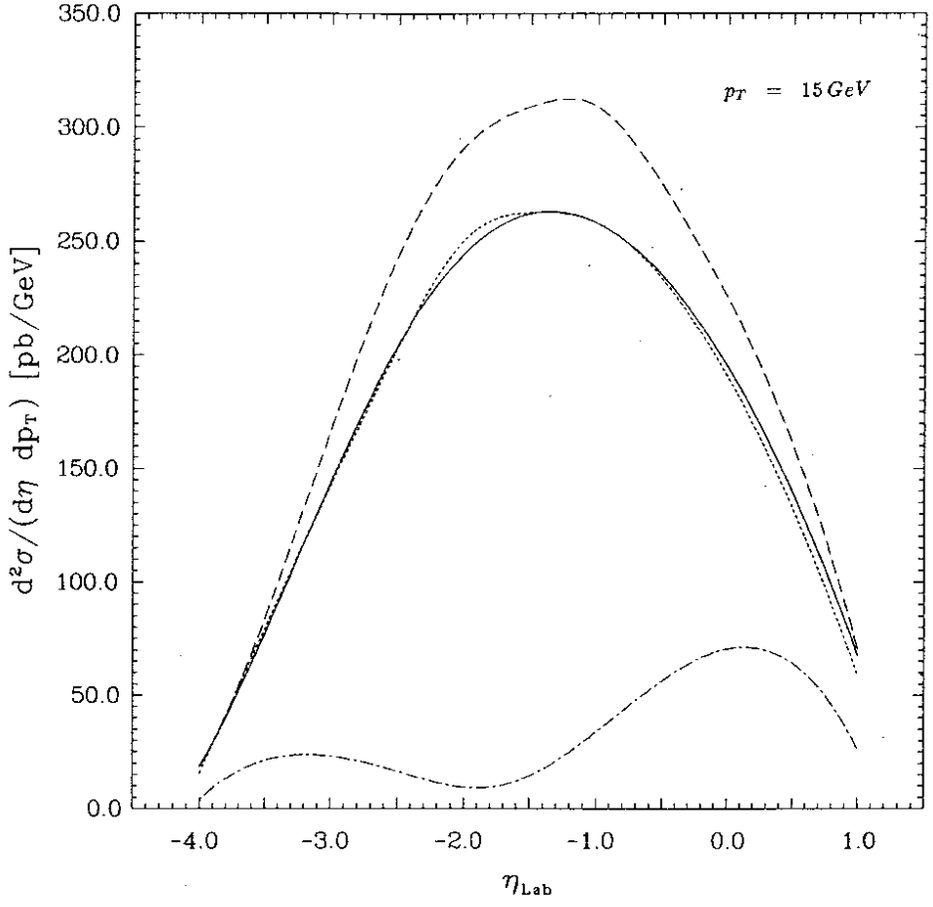
350.0
300.0
250.0
200.0
150.0
100.0
50.0
0.0
-4.0
-3.0
-2.0
-1.0
0.0
1.0
$p_T = 15\,GeV$
$d^2\sigma/(d\eta\ dp_T)$ [pb/GeV]
η_{Lab}

Fig. 3b

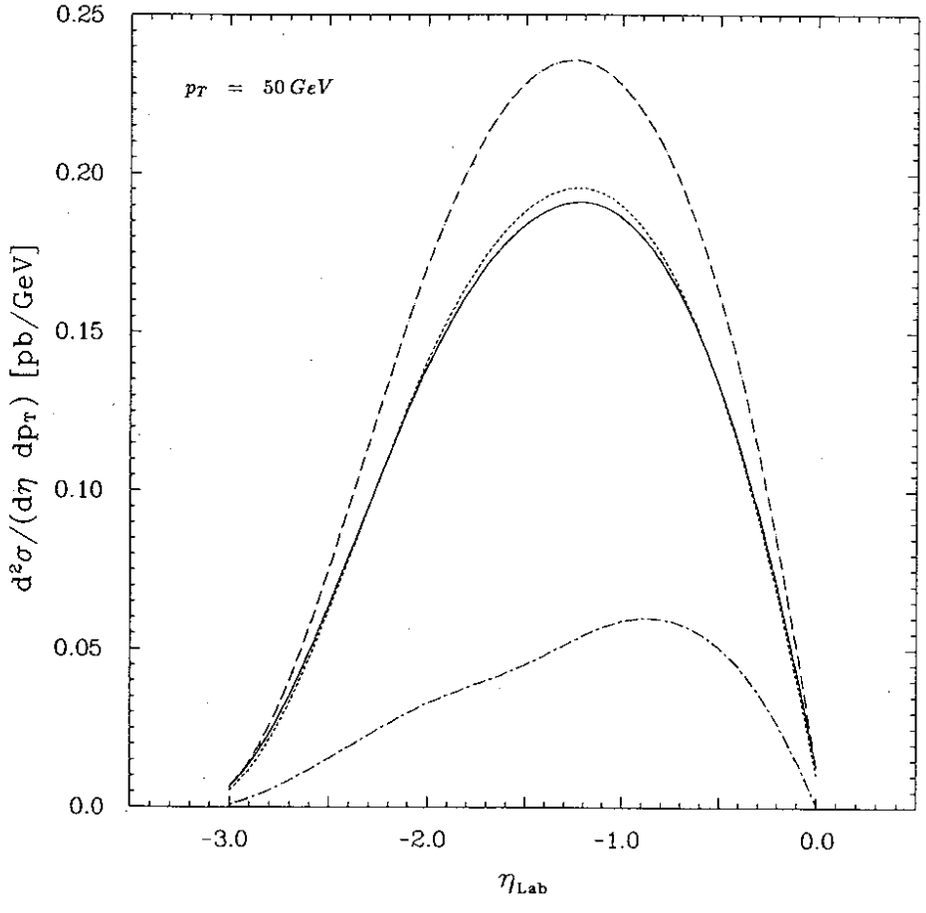
p_T = 50 GeV
0.25
0.20
0.15
0.10
0.05
0.0
$d^2\sigma/(d\eta\ dp_T)$ [pb/GeV]
-3.0
-2.0
-1.0
0.0
η_{Lab}

Fig. 3c

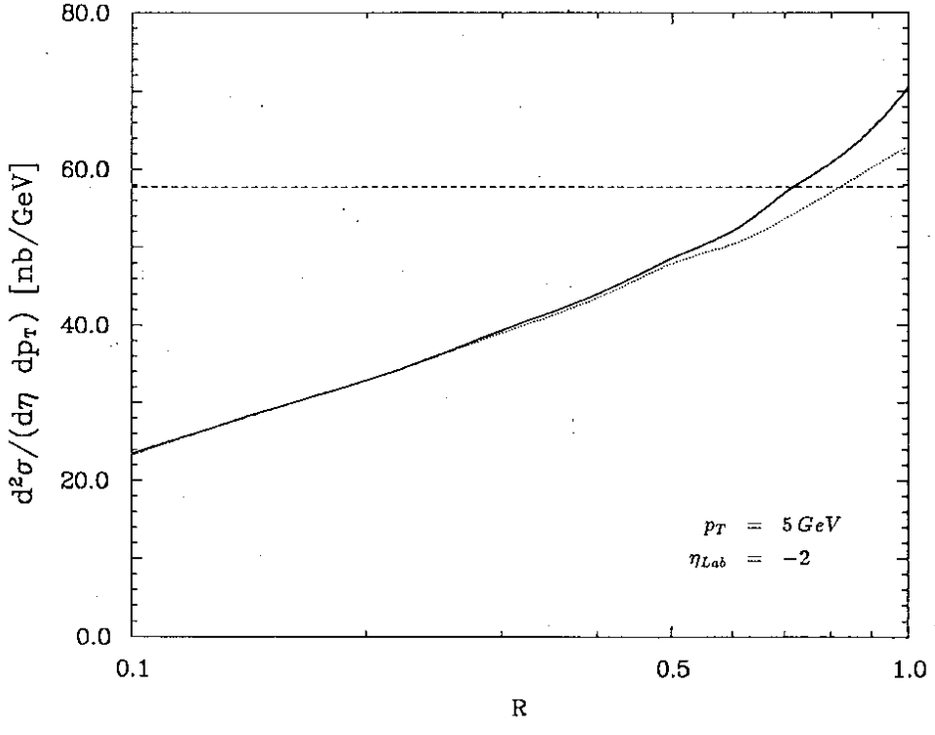
80.0
60.0
40.0
20.0
0.0
$d^2\sigma/(d\eta\ dp_T)$ [nb/GeV]
p_T = 5 GeV
η_{Lab} = −2
0.1
0.5
1.0
R

Fig. 4a

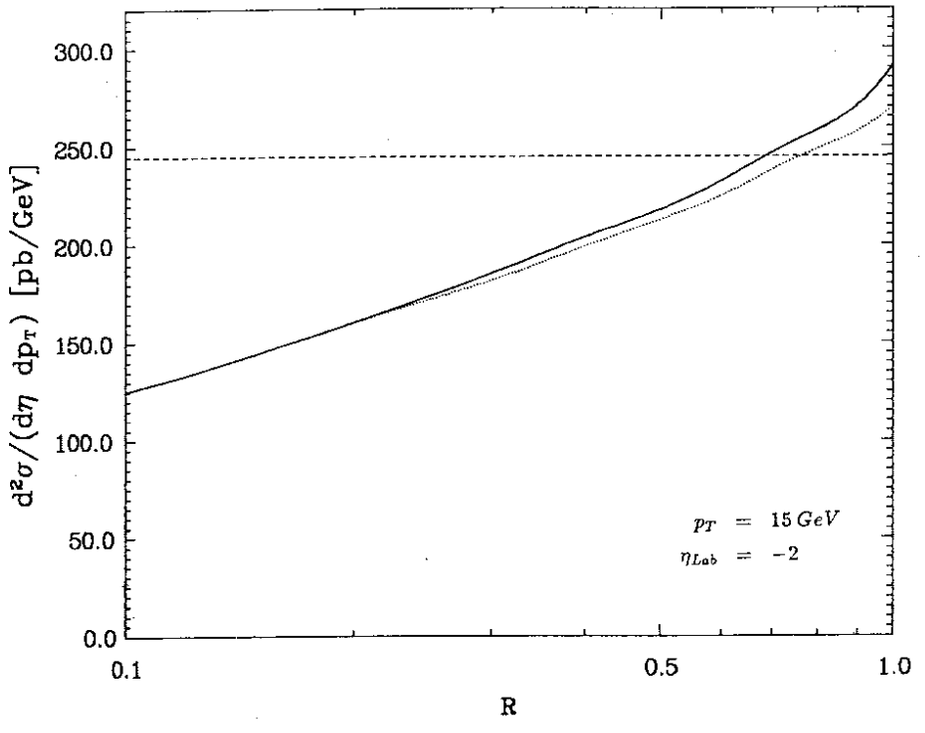
300.0
250.0
200.0
150.0
100.0
50.0
0.0
0.1
0.5
1.0
R
$d^2\sigma/(d\eta\ dp_T)$ [pb/GeV]
$p_T = 15\,GeV$
$\eta_{Lab} = -2$

Fig. 4b

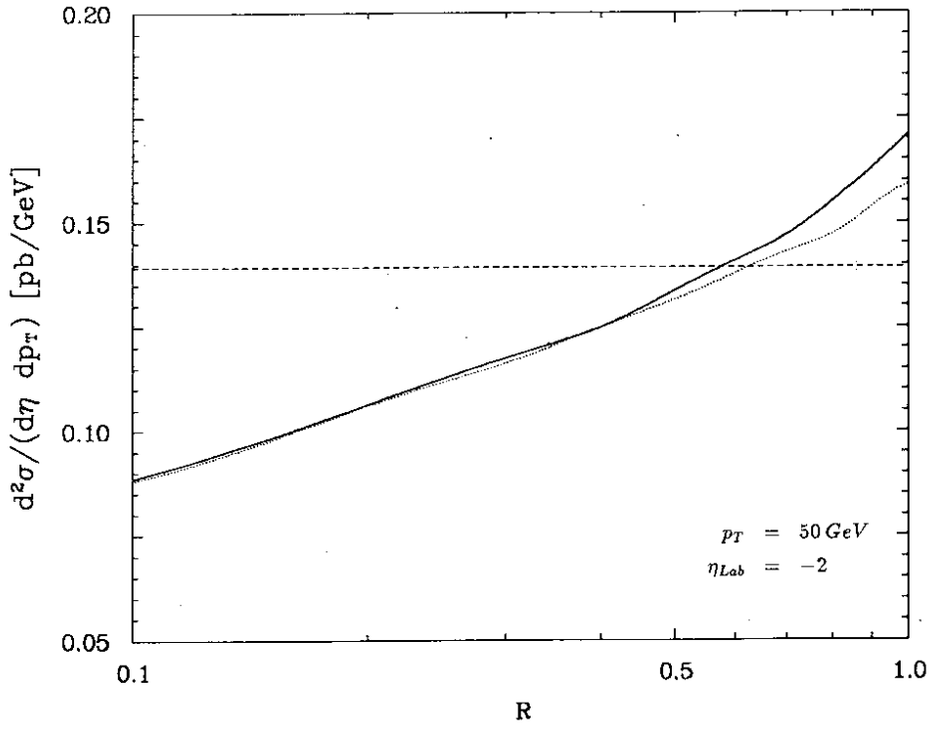
0.20
0.15
0.10
0.05
0.1
0.5
1.0
R
$d^2\sigma/(d\eta\ dp_T)$ [pb/GeV]
$p_T = 50\,GeV$
$\eta_{Lab} = -2$

Fig. 4c

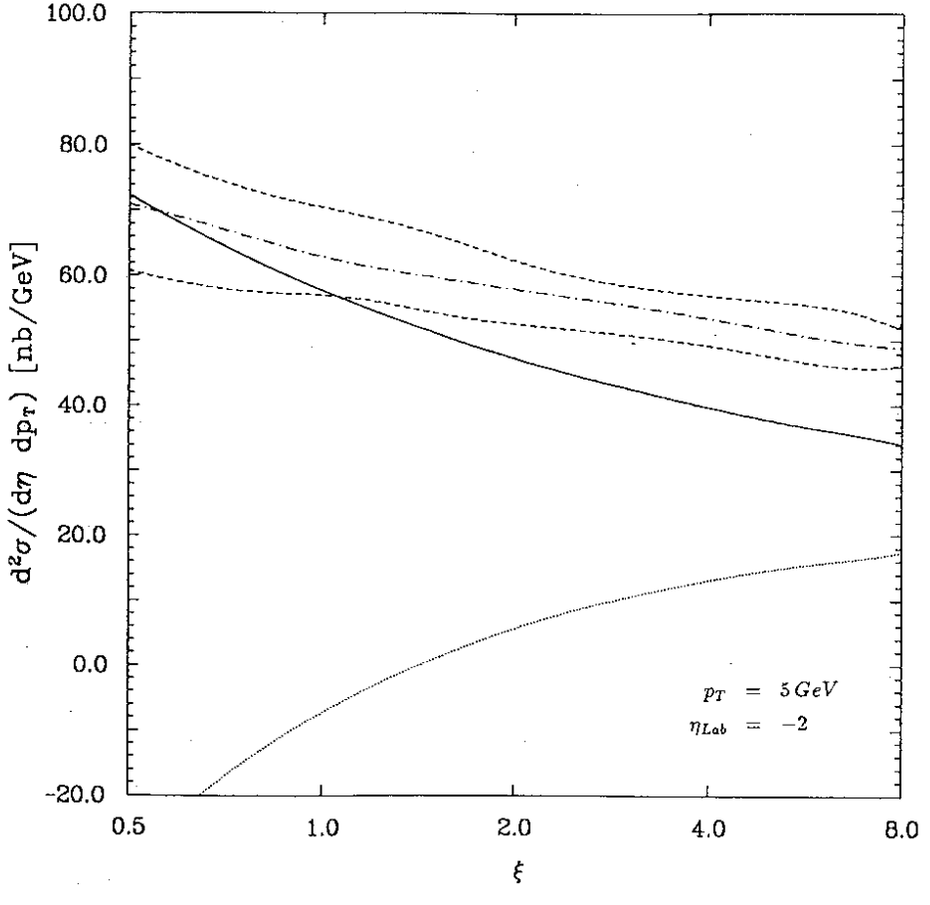
100.0
80.0
60.0
40.0
20.0
0.0
-20.0
0.5
1.0
2.0
4.0
8.0
$d^2\sigma/(d\eta\ dp_T)$ [nb/GeV]
ξ
$p_T = 5\,GeV$
$\eta_{Lab} = -2$

Fig. 5a

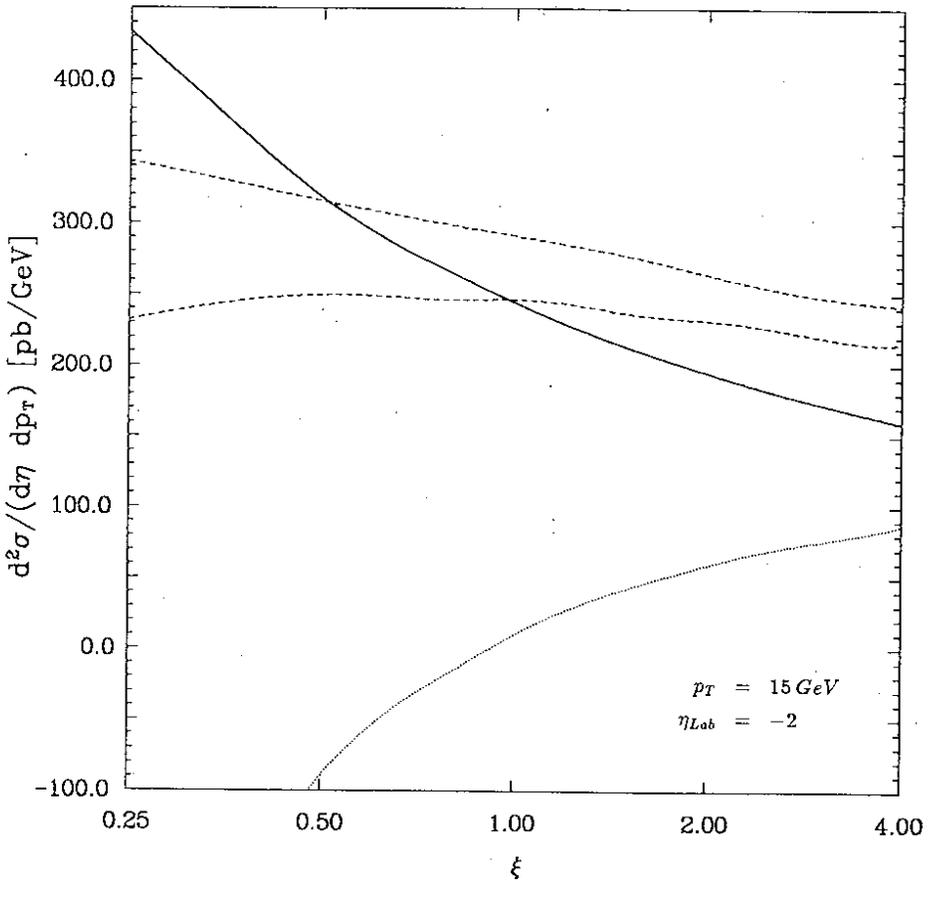
400.0
300.0
200.0
100.0
0.0
-100.0
0.25
0.50
1.00
2.00
4.00
$d^2\sigma/(d\eta\ dp_T)$ [pb/GeV]
ξ
$p_T = 15\,GeV$
$\eta_{Lab} = -2$

Fig. 5b

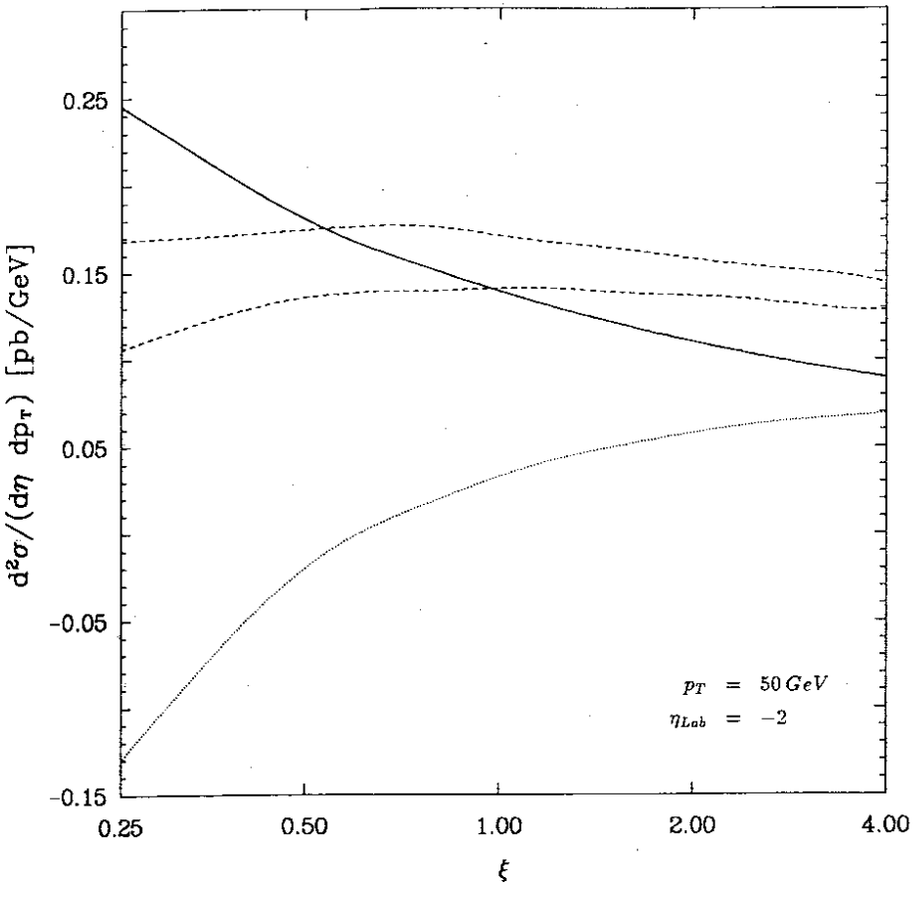
0.25
0.15
0.05
-0.05
-0.15
0.25
0.50
1.00
2.00
4.00
ξ
d²σ/(dη dp_T) [pb/GeV]
p_T = 50 GeV
η_Lab = −2

Fig. 5c